Editors' Suggestion

Assignment of excitonic insulators in *ab initio* theories: The case of $NiBr_2$

Stefano Di Sabatino [1,*] Alejandro Molina-Sánchez [2,†] Pina Romaniello [1,‡] and Davide Sangalli [3,§]

[1] *Laboratoire de Physique Théorique, CNRS, Université Toulouse III (UPS), 118 Route de Narbonne, F-31062 Toulouse, France and European Theoretical Spectroscopy Facility (ETSF)*

[2] *Institute of Materials Science (ICMUV), Universitat de València, Catedrático Beltrán 2, E-46980, Valencia, Spain*

[3] *Istituto di Struttura della Materia, Consiglio Nazionale delle Ricerche (CNR-ISM), Via Salaria Km 29.5, CP 10, I-00016 Monterotondo Stazione, Italy and European Theoretical Spectroscopy Facility (ETSF)*

(Received 21 December 2022; revised 17 February 2023; accepted 22 February 2023; published 9 March 2023)

In this work we perform a detailed first-principles analysis of the electronic and optical properties of $NiBr_2$ within the state-of-the-art GW+BSE scheme to determine whether this system displays negative excitonic energies, which would identify it as an (half) excitonic insulator. Particular attention is paid to the convergence of the GW band structure and to the consistency between approximations employed in the ground-state calculations and approximations employed in the linear response calculations. We show that these two issues play a crucial role in identifying the excitonic nature of $NiBr_2$.

DOI: 10.1103/PhysRevB.107.115121

I. INTRODUCTION

The seminal paper [1] of Jerome and coworkers predicted the realization of the broken-symmetry excitonic insulator (EI) phase in materials where the exciton binding energy overcomes the fundamental band gap. The phase transition from a symmetric state to the lower-symmetry EI would be purely electronically driven. A very rich activity followed, with various research groups trying to find signatures of the EI phase in different classes of materials, ranging from semimetals to small gap semiconductors and nanostructures [2–16].

The determination of the EI phase is mostly quantitative, rather then qualitative, i.e., it relies on the relative value of the excitonic binding energy versus the fundamental band gap. Therefore accurate numerical simulations are essential. Moreover, the broken-symmetry phase is often associated to an instability of the crystal structure, and a distortion towards a lower symmetry phase [9,14,17]. It then becomes a chicken and egg question whether it is the lattice distortion that drives the electronic phase transition or vice versa, and whether or not one should speak about excitonic instability at all in many cases. The structural and the electronic phase transitions cannot be disentangled experimentally, making a direct proof of the EI existence a nontrivial problem, with different experimental groups often reaching opposite conclusions. This is why *ab initio* numerical simulations are the key instrument to be used. Indeed, while indications of the EI phase from experimental measurements have been collected, in most works the assignment of the EI phase is based on *ab initio* numerical simulations, either as support of experimental data or as purely theoretical/computational works.

The state-of-the-art approach to model excitons in *ab initio* simulations is the so-called Bethe-Salpeter equation (BSE), computed on top of an accurate band structure including quasiparticle GW corrections, within the so-called GW+BSE scheme. Then, numerically, a material is foreseen to be an excitonic insulator if the BSE binding energy overcomes the GW band gap. This approach has been used in several works [7,8,11,12,18]. Recently, following this approach, a possible EI phase was identified by Jiang *et al.* [18] for the magnetic layered $NiBr_2$. $NiBr_2$ is quite unique for two reasons. First of all, it has a very large band gap (about 4 eV), compared to other materials explored so far. This would suggest that the EI phase could be ruled out from the beginning, since typical exciton binding energies range from few meV to few hundreds meV in bulk materials. Second, $NiBr_2$ is magnetic, thus leading to an interplay between charge and spin degrees of freedom. As a result, the EI phase was predicted to be realized in one spin channel only. The authors referred to this case as a half-EI (HEI).

The GW+BSE scheme is a well-established numerical scheme, and it works surprisingly well in describing the optical properties of a wide range of materials, ranging from bulk insulators and semiconductors, to layered and two-dimensional (2D) materials, 1D materials, such as carbon nanotubes, up to isolated systems such as clusters and molecules. In $NiBr_2$, similarly to other EI candidates, the GW+BSE scheme results in solutions of the excitonic Hamiltonian with slightly negative energies (few meV below zero). However, the validity of the GW+BSE scheme to correctly capture poles with energy close, or even below, zero should be questioned from the beginning for various reasons. First, it is well known that the results of the GW+BSE scheme depend on the starting point, i.e., on the functional employed in the initial density functional theory (DFT) calculation. For

*stefano.disabatino@irsamc.ups-tlse.fr
†alejandro.molina@uv.es
‡pina.romaniello@irsamc.ups-tlse.fr
§davide.sangalli@ism.cnr.it

example, if the initial band structure is computed starting from a DFT calculation using the PBE or the PBE0 approximation, one should refer to it as *GW*@PBE+BSE or *GW*@PBE0+BSE, respectively. Although a change of the functional might only result in small energy shifts, this could be enough to move an energy eigenvalue of the BSE across zero. Second, in this protocol approximations employed in the ground-state calculations are not consistent with the approximations used in the linear response part. As a consequence, for example, the *GW*@DFT+BSE scheme, if used to compute excitations in the spin flip channel, fails in reproducing the Goldstone sum rule for magnons, i.e., it fails to give a zero-energy pole in magnetic materials [19]. This failure is independent of the DFT flavor, the corresponding error can be large, and it clearly shows that the scheme is not reliable for poles with energy close to zero. A similar inconsistency is also at the origin of the incorrect long-wavelength limit of the plasmon energy within *GW*@BSE [20].

Surprisingly, these issues have been discussed very little in the literature when addressing the existence of possible EI phases. In the present paper we use the quite unique case of $NiBr_2$ to address this deficiency. We show that $NiBr_2$ is an extreme case where one should be very careful in proposing the existence of an EI phase, since the state-of-the-art *GW*@DFT+BSE scheme is so much affected by the starting point that even qualitatively results can change completely. These findings are not specific to the case of $NiBr_2$ but can be extended to the analysis of a wide range of materials.

The paper is organized as follows. In Sec. II we define in a clear way what an EI phase (or an EI instability) is, and discuss the numerical protocols, which properly address the existence of the EI phase in general. In particular we discuss why one has to be consistent in the approximations used to describe the ground state and the response of the system. In Sec. III we present the results of our numerical simulations and discuss the band structure (Sec. III A) as well as the absorption spectrum (Sec. III B) of ferromagnetic $NiBr_2$ using various approximations. We finally draw our conclusions and perspectives in Sec. IV.

II. THEORETICAL PROTOCOL

The EI phase has two fundamental key properties: (i) it is a broken-symmetry phase of electronic nature, and (ii) it is described by introducing the long-range electron-hole interaction in the simulations. These are the two essential requirements that any numerical simulation predicting an EI phase should take into account.

Let us define the electronic Hamiltonian H, which also includes the potential of the atoms in a chosen crystal lattice structure, and its eigenvalues (at fixed electron number) E_λ, with E_0 the ground-state energy. We can define a corresponding point symmetry group S and a group of discrete translations T, such that $[H, S] = 0$ and $[H, T] = 0$. We call Ω^{ST} the phase space of electronic states, which respect such symmetry groups, Ω the global phase space, and Ω^S (Ω^T) the phase space, which respects the S (T) group alone. We have $\Omega \supseteq \Omega^S \supseteq \Omega^{ST}$ ($\Omega \supseteq \Omega^T \supseteq \Omega^{ST}$). The excitonic insulator phase arises from a spontaneous symmetry breaking. In the present paper we will focus on the spontaneous symmetry breaking with respect to the S group, in line with the study carried out in Ref. [18]. We notice that $NiBr_2$ is an indirect gap material (although with a very small difference between direct and indirect gap, as we shall see), and possibly finite momentum excitons are those of minimum energy. Indeed the existence of a spin spiral/cycloidal spin structure has been predicted [21–23], which could be explained as due to an instability connected to finite momentum excitons. It would be interesting to address this issue in a future work. Accordingly, we define E_0^{ST} as the global energy minimum over Ω^{ST}, and E_0^T as the global energy minimum over Ω^T. A broken-symmetry phase ground state exists if and only if $E_0^T < E_0^{ST}$.

Standard *ab initio* simulations compute the ground state with the symmetry specified by the crystal lattice structure of the system, within a given approximation for the exchange and correlation (XC) energy; we indicate the corresponding total energy as E_0^{ST,XC_g}, with XC_g referring to the XC approximation used in the ground state. There are then two options available to check if a broken-symmetry state with energy $E_0^{T,\mathrm{XC}_g} < E_0^{ST,\mathrm{XC}_g}$ exists: (i.1) to perform a second ground-state simulation without symmetry or (i.2) to compute the spectrum of the neutral excitations of the material, $\omega_\lambda = (E_\lambda - E_0)$, at zero transferred momentum.[1] In the latter case there is no need to impose symmetry breaking. Indeed, neutral excitations are computed from the solution of the linear response function $\chi(\omega)$. The excited-state energies, E_λ, and the corresponding wave functions, Ψ_λ, which appear in the Lehmann representation of $\chi(\omega)$, do not belong to Ω_{ST} in general. More precisely, given the space symmetry group S, the states Ψ_λ can be classified as degenerate multiplets of the irreducible representations R_S^λ of the space group. Symmetry operations of Ω_{ST} can in general send a state of a given multiplet into any other state of the same multiplet. Because of that, the states of a monodimensional representation R_S^λ are singlets, i.e., nondegenerate, and belong to Ω_{ST}. Instead, states of a multidimensional representations R_S^I do not belong to Ω_{ST}, and they must be considered together to obtain a closed subspace with respect to the symmetry operation of the group S. If a multiplet of states has energy lower than the ground state, then a spontaneous symmetry breaking would be favored, with an emerging ground state composed by a random linear combination of the states in the multiplet.

If option (i.1) is chosen, the same level of approximation must be used in the ground-state calculation with and without symmetry. Comparing $E_0^{T,\mathrm{XC}_{g1}}$ and $E_0^{ST,\mathrm{XC}_{g2}}$, with XC_{g1} and XC_{g2} two different XC approximations used in the ground state, does not have any validity. Moreover, the long-range electron-hole interaction needs to be considered. In some works the EI phase has been studied on the basis of calculations using the local density approximation (LDA) or the generalized gradient approximation (GGA), i.e., $\mathrm{XC}_g = \mathrm{LDA/GGA}$ [14,24]. While also within these approximations a symmetry-broken phase could be obtained,

[1]The finite momentum excitations would describe the breaking of the translational symmetries as well. We do not consider this case here.

such phases should not be labeled as EI, since LDA/GGA completely miss the long-range behavior of the electron-hole interaction. Indeed, it is well known that time-dependent DFT (TDDFT), within the LDA or GGA approximations (TDLDA or TDGGA), cannot describe excitons in the excited states, and thus these approximations cannot capture the EI phase in the ground state either.

In case option (i.2) is chosen, the total energy of possible broken-symmetry phases can be obtained by defining $E_\lambda^{T,\mathrm{XC}} = E_0^{ST,\mathrm{XC}_g} + \omega_\lambda^{ST,\mathrm{XC}_e}$, with $\omega_\lambda^{ST,\mathrm{XC}} = E_\lambda^{T,\mathrm{XC}} - E_0^{ST,\mathrm{XC}}$ a zero-momentum neutral excitation of the system, using consistent approximations between ground-state (XC_g) and excited-state (XC_e) calculations. Then the criteria to establish the existence, for some λ_0, of a broken-symmetry phase becomes $\omega_{\lambda_0}^{ST,\mathrm{XC}_e} < 0$. In such situation we can identify $E_{\lambda_0}^{T,\mathrm{XC}} = E_0^{T,\mathrm{XC}}$ as the global ground-state energy. The state-of-the-art scheme to describe excitons in the *ab initio* framework is BSE. $\omega_\lambda^{\mathrm{XC}_e} < 0$, with XC_e referring to the XC approximation used for the BSE kernel, is then often used as the gold standard to predict the existence of the excitonic insulator phase. Within this approach the essential consistency condition at the core of option (i.2) would rely on the use of a one-body Green's function, which is a self-consistent solution of the Dyson equation for a given self-energy approximation and on the use of the same level of approximation for the self-energy and the BSE kernel [19].

However, in practical calculations, this consistency condition is violated since the state-of-the-art is the *GW*@DFT+BSE scheme. Within this scheme the BSE kernel is obtained from the Hartree plus screened-exchange self-energy (HSEX) approximation, i.e., $\mathrm{XC}_e = \mathrm{HSEX}$, while $\mathrm{XC}_g = GW@\mathrm{DFT}$. Ideally, one would use full self-consistency including vertex corrections in the ground state and the corresponding (frequency-dependent) kernel in the BSE. This is, however, time consuming and, moreover, it would require a dynamical kernel in the BSE, which is not yet a standard feature. There is also a more fundamental problem, which is related to the fact that by including higher-order corrections to *GW* there are more and more ways of iterating the equations and hence an increased danger of running into unphysical solutions [25–27]. One can then stick to the *GW* approximation, but, again, this would require a BSE with a dynamical kernel. To be consistent within the standard BSE implementations possible choices for the self-energy are HSEX and COHSEX (Coulomb hole+screened exchange), with or without a fixed screened Coulomb interaction in the self-consistent procedure [19,28,29] (if one neglects second-order corrections in W in the BSE kernel). For example fully self-consistent COHSEX has been shown to substantially reduce the violation of the Goldstone-mode condition (see, e.g., Ref. [28]). Even ignoring this point and assuming that *GW* is a good starting point for a BSE calculation, at least an eigenvalue self-consistent *GW* (ev*GW*) procedure should be carried out. However, this would not eliminate the starting point dependence, which, as we will see, is of crucial importance in the present study. However, both self-consistent HSEX and ev*GW* can be very demanding. An alternative path is to use DFT with hybrid functionals, which are computationally affordable. Hybrid functional simulations include (a fraction of) the long–range electron-hole interaction and can be used to capture EI phases. In this case $\mathrm{XC}_g = \mathrm{XC}_e = \mathrm{hybrid}$ can be used, by employing TDDFT for the excited states. To underline this consistency, we will use here the notation PBE0+TDPBE0 for example for the PBE0 case. Indeed, it has been shown that hybrid functionals can capture excitonic excited states [30] and EI phases [9]. In general the exchange fraction entering hybrids is not properly screened, and this could be particularly problematic in 2D materials, since the 2D nature of the screening is completely missing. Nevertheless, as we will see, it remains a valid approach to demonstrate the concept of consistency we discussed above.

In this work we will adopt the protocol described in option (i.2) to identify possible EI phases in $NiBr_2$ and we will calculate the optical spectrum within *GW*@PBE+BSE, *GW*@PBE0+BSE and PBE0+TDPBE0. This will allow us to address both the starting-point dependence of the *GW*@DFT+BSE scheme and to consider a proper scheme with $\mathrm{XC}_g = \mathrm{XC}_e$.

III. RESULTS

We studied monolayer $1T$-$NiBr_2$ in its ferromagnetic ground state. Density functional theory calculations were performed using the QUANTUM ESPRESSO code [31] within both the Perdew-Burke-Ernzerhof (PBE) and the PBE0 exchange correlation functional [32]. Optimized norm-conserving Vanderbilt pseudopotentials have been generated using ONCVPSP [33]. The self-consistent (SCF) simulations converged with an energy cutoff of 80 Ry and a $\mathbf{k}$-point grid of $9 \times 9 \times 1$ (the direct band gap at Γ has been converged to 0.01 eV).

We then used the DFT wave functions $\psi_{n\mathbf{k}}^{KS}(\mathbf{r})$ and energies $\epsilon_{n\mathbf{k}}^{KS}$ to perform *GW* and BSE simulations. For the PBE case we recomputed $\psi_{n\mathbf{k}}^{KS}(\mathbf{r})$ and $\epsilon_{n\mathbf{k}}^{KS}$ with a non-self-consistent (NSCF) calculation on a $19 \times 19 \times 1$ $\mathbf{k}$-point grid in the Brillouin zone. For the PBE0 case instead we used a $9 \times 9 \times 1$ $\mathbf{k}$-point grid. This is due both to the higher computational cost of PBE0 and to the fact that, with the code used in the present work (QUANTUM ESPRESSO), it is not possible, in the case of hybrid functionals, to use different $\mathbf{k}$-point grids in the NSCF and SCF calculations. As we shall see, this restriction does not affect our conclusions. We computed the one-shot *GW* quasiparticle (QP) corrections on top of DFT using the Yambo code [34,35]. Dynamical screening effects have been taken into account using the Godby-Needs plasmon-pole approximation (PPA) [36]. Both in DFT and, successively, in *GW* and BSE, we used a slab model with a 40 a.u. vacuum thickness. Moreover, the Coulomb cutoff technique [37] has been used to ensure no interactions between periodic images. In the *GW* step, we used a cutoff of 40 Ry for the input variable FFTGvecs, which determines the size of the real-space grid and the energy cutoff for the wave functions; an energy cutoff four times bigger, i.e., of 320 Ry, for V_{XC} and for the exchange part of the self-energy Σ_x; finally an energy cutoff of 10 Ry for the screening and the correlation parts of the self-energy Σ_c We included a total of 200 bands in the screening and 500 in the evaluation of the self-energy. Note that to guarantee converged results we use the extrapolation procedure explained in the Supplemental Material [38]. In the optical response we took into account excitonic effects

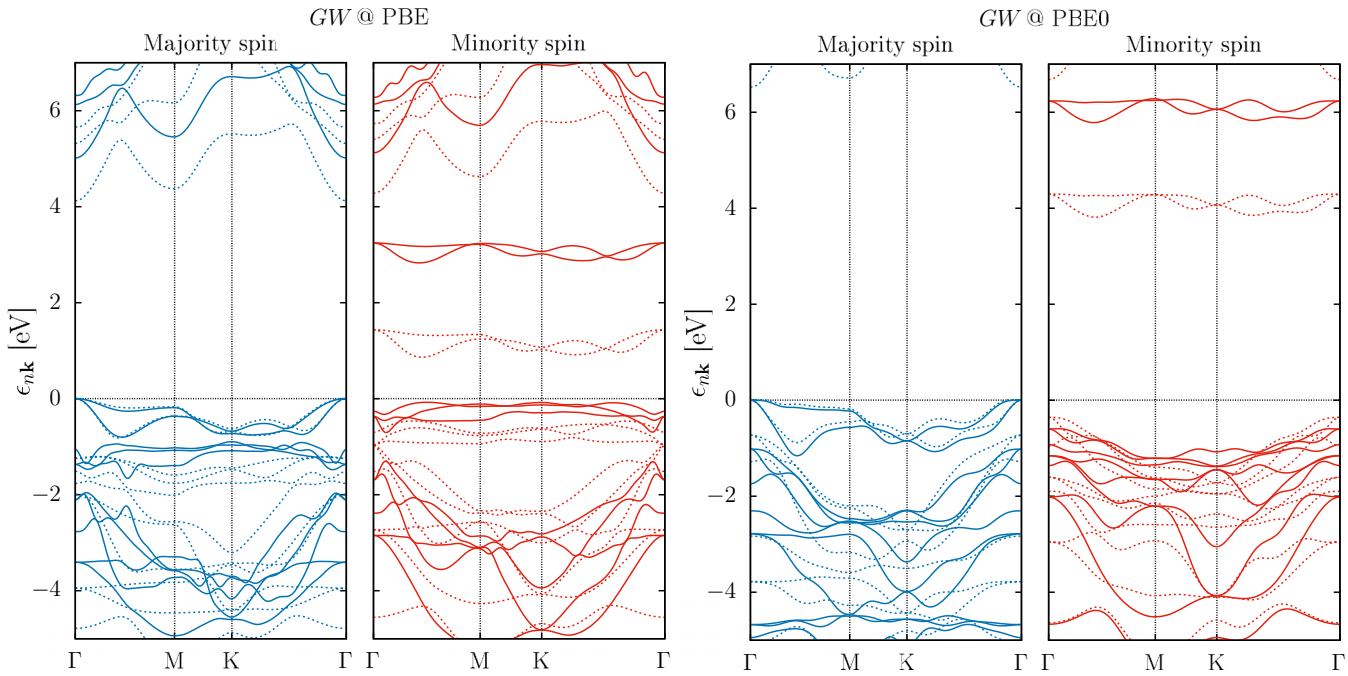

FIG. 1. Spin-resolved band structure (majority- and minority-spin channels are reported in blue and red, respectively) for *GW*@PBE (left) and *GW*@PBE0 (right) are reported with a continuous line. The DFT band structures used as starting point for the *GW* correction are reported with a dashed line. Energy zero is at the top of valence band.

via the Bethe-Salpeter equation [39,40]. The BSE absorption spectrum has been calculated using a static screening converged using the same parameters of the *GW* calculation. We used a cutoff of 4 Ry for the electron-hole exchange and 10 Ry for the screened interaction. We included bands 7–23 to obtain a converged spectrum up to 10 eV.

In the following we demonstrate that the occurrence of negative energy solutions of the BSE strongly depends on the choice of the approximations used in the ground state and for the BSE kernel. In particular the lack of self-consistency in the *GW* band structure and of consistency between ground-state approximations and BSE kernel approximations can lead to a questionable EI phase.

We notice that, besides the consistency between the approximations used for the ground state and for the linear response and the role of the starting point, another possible source of error is the static approximation for the screening adopted in standard BSE calculations, which may not be justified in cases where low-energy excitations or negative energy instabilities are sought [41,42]. We will not address this issue in the present work, since, at least for extended systems, there is not yet implementation of the BSE with a dynamical kernel.

A. Band structure

The starting point for a BSE calculation is a single-particle band structure obtained correcting the DFT energies. The approximation chosen for the DFT determines the quality of the screened interaction W, which is computed within the RPA approximation using Kohn-Sham energies. This results in the so-called W_0 screened interaction. W_0 enters the one-shot *GW* or G_0W_0 approach, which is usually employed for the band structure. The one-shot *GW* is also employed in the present work. Even without invoking self-consistency, *GW* calculations can be problematic in 2D materials. We found, indeed, that, for the system under study, particular attention has to be paid when converging the *GW* quasiparticle corrections. See also the discussion in the Supplemental Material [38] (see, also, Refs. [43,44] therein).

In Fig. 1 we show PBE and PBE0 spin-resolved band structures, separated in majority (M) and minority (m) spin channels. The corresponding *GW*@PBE and *GW*@PBE0 band structures are also shown. In all cases the band gap is indirect, with 0.83 eV at the PBE level compared to 3.79 eV at the PBE0 level, and it is due to transitions from the majority valence band maximum (VBM) at Γ towards the minority conduction band minimum (CBM), which is at roughly half-way along the ΓM high symmetry line. Also the direct band gaps within PBE0 (4.45 eV and 6.52 eV for m-m and M-M spin channels, respectively) are significantly larger than the ones obtained using PBE (1.33 eV and 4.09 eV for m-m and M-M spin channels, respectively). This is expected due to the fraction of HF exchange taken into account in the PBE0 functional.

Moving to *GW*, one would naively expect that, despite the starting-point dependence, the *GW*@PBE and *GW*@PBE0 gaps should be close to each other, with *GW*@PBE approaching the expected self-consistent *GW* result from below, i.e., with the *GW* corrections opening the PBE gap, and with *GW*@PBE0 from above, i.e., with the *GW* corrections closing the PBE0 gap. However, this is clearly not the case as shown in Fig. 1. *GW*@PBE opens the PBE gap from 0.83–2.62 eV. Direct band gaps are increased to 2.91 eV and 5.01 eV for the minority and majority spin channels, respectively. However, *GW*@PBE0 also opens the PBE0 gap from 3.79–5.75 eV. Direct band gaps are 6.56 eV and 7.41 eV for the minority

TABLE I. Indirect and direct band gaps (in eV).

	PBE	PBE0	*GW*		
	[44]		@PBE	@PBE [44]	@PBE0
ind. gap M-m	0.83	0.88	3.79	2.82	2.62	5.75
dir. gap m-m	1.33	1.34	4.45	2.91	2.62	6.56
dir. gap M-M	4.09	3.95	6.52	5.01	5.37	7.41
dir. gap M-m	0.99	1.04	3.86	3.05	3.06	5.91

and majority spin channels, respectively. See also Table I for a comparison of all values. This clearly points to the fact that W_0^{PBE} and W_0^{PBE0} are different and that, accordingly, the two G_0W_0 self-energies are different. One can then wonder which result is the most reliable.

On one hand the *GW* @PBE is the state-of-the-art scheme to compute quasiparticle band structure. Indeed, the PBE screening entering W_0^{PBE} is usually a reasonable approximation to the physical screening due to error cancellations between (i) the underestimated fundamental gap, and (ii) the neglected excitonic effects. On the other hand hybrid functionals such as PBE0 are expected to better approximate quasiparticle wave functions and energies. Also simulations based on the hybrid HSE0 functional [18,45] give a band structure rather close to the PBE0 band structure. However, *GW* @hybrids, despite being very promising [46–48], as for example in the case of hybrid-organic perovskite materials [47], is a scheme, which has not been much tested yet, since the compatibility of *GW* codes with hybrid functionals is a quite recent feature. By correcting the electronic gap, hybrid functionals tend to underestimate the electronic screening, which may result in a overestimation of the *GW* @hybrids gap [46]. Indeed, in $NiBr_2$ the underestimated screening leads to a very strong exchange term, even bigger than the exchange fraction entering in PBE0. As a consequence, it is more reasonable to directly compare *GW* @PBE with hybrids such as PBE0. The estimated experimental band gap, probed using STS on $NiBr_2$ thin films, down to the monolayer, ranges between 3.4 and 4.5 eV, in good agreement with the PBE0 value [49].

Besides this evident but yet quantitative difference, there is a more important qualitative difference between PBE and PBE0 band structures, which is also inherited by the corresponding *GW* band structure. Within PBE there exist three almost flat bands in the minority channel, which are very close in energy to the top of the valence band in the majority spin channel. These bands are nickel $3d$ states [18], in particular with t_{2g} character, which are likely not well described within PBE. Indeed, they are not present within our PBE0 simulations, nor in the HSE0 and LDA+U results in the literature [18,45]. Moving to *GW* @PBE these same states remain there, pointing to the fact that the PBE wave functions are not well described, and that PBE is not a good starting point. These states also show a quite peculiar behavior in the *GW* simulations, and, as we shall see, they are responsible for the very sharp difference in the spectrum of *GW* @PBE+BSE compared to PBE0+TDPBE0 or *GW* @PBE0+BSE. In the Supplemental Material [38] we discuss the convergence of the *GW* @PBE quasiparticle corrections. We highlight the unusual behavior of these flat Ni $t_{2g\downarrow}$ bands, and we discuss in detail the very slow convergence compared to the energy cutoff used in the description of the screened interaction. The discussion agrees with previous numerical studies [50], although this fact has been somehow overlooked in past simulations on 2D materials [18]. Indeed *GW* @PBE corrections on these occupied Ni $t_{2g\downarrow}$ states lead to a situation in which the majority and the minority VBM are very close in energy (during the *GW* convergence their relative position is even inverted). The direct gap switches character, from M-m to m-m, and the system almost becomes a direct gap material with an energy difference between *GW* @PBE direct and indirect gap of 9 meV (compared to 500 meV in PBE, 660 meV in PBE0, and 810 meV in *GW* @PBE0). The small m-m gap is also part of the reason why negative poles will appear in the response function calculated at the level of *GW* @PBE+BSE, as we will discuss in Sec. III B.

The conclusion of this analysis is that $NiBr_2$ is an indirect band gap semiconductor. The indirect gap is majority-minority, as expected in standard magnetic materials. Looking at the direct gap, this is also majority-minority, the minority-minority gap is slightly larger (less than 1 eV), while the majority-majority gap is significantly larger. This behavior is due to the empty spin-minority Ni $3d$ orbitals, with e_g character, which lie in between the more predominantly p-like valence and conduction bands.

B. Optical properties

We now turn our attention to the optical properties of $NiBr_2$. In Fig. 2 the *GW* @PBE+BSE absorption spectrum is reported together with the *GW* @PBE0+BSE and the PBE0+TDPBE0 spectra. All spectra are dominated by an intense excitonic peak, which we label E_0. All methods describe E_0 as an exciton mostly located nearby Γ in the BZ (see Fig. 3) and corresponding to a transition from p bands $\epsilon_{p\mathbf{k}\downarrow}$ to $d(e_g)$ bands $\epsilon_{d\mathbf{k}\downarrow}$ in the spin minority channel. At energy larger then E_0 the spectral intensity is strongly reduced and eventually it goes up again at even larger energy. The position of the E_0 peak shifts from 3.3 eV (*GW* @PBE+BSE), to 3.6 eV (PBE0+TDPBE0), and to 4.1 eV (*GW* @PBE0+BSE). The E_0 energy is always lower compared to the $(\epsilon_{d\mathbf{k}\downarrow} - \epsilon_{p\mathbf{k}\downarrow})$ energy difference. We define its binding energy $b_{E_0} = \min_{\mathbf{k}}(\epsilon_{d\mathbf{k}\downarrow} - \epsilon_{p\mathbf{k}\downarrow}) - E_0$. $b_{E_0} \approx$ 1 eV in both *GW* @PBE+BSE (1.1 eV) and PBE0+TDPBE0 (0.9 eV), while $b_{E_0} = 2.4$ eV for *GW* @PBE0+BSE. This discrepancy is again due to the underestimated RPA screening obtained using the PBE0 starting point. This leads to an overestimation of the band gap, which is here compensated by an overestimation of the binding energy and results in a peak position not very different from *GW* @PBE+BSE and PBE0+TDPBE0. As for the band structure case, the conclusion here is that it is better to directly compare *GW* @PBE+BSE to PBE0+TDPBE0.

The qualitative behavior of the spectrum is instead significantly different at energy below E_0. All methods show poles at energy well below E_0, due to transitions between occupied and flat bands in the minority spin channel, which we identify as $d(t_{2g})$ states (see Supplemental Material [38]), and the empty spin minority $d(e_g)$ states. However, within

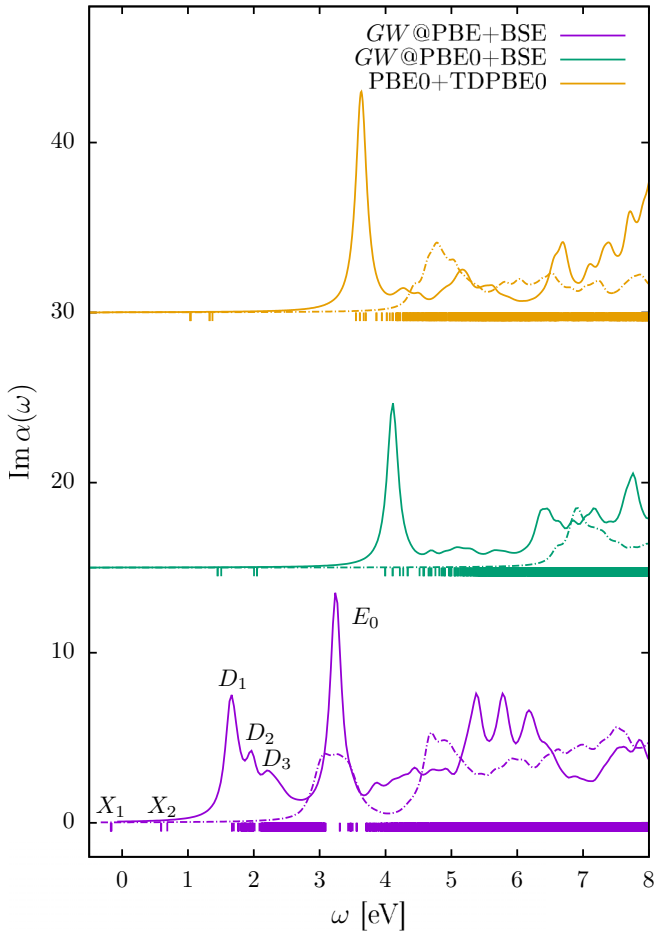

FIG. 2. Imaginary part of the macroscopic polarizability calculated within *GW*@PBE+BSE (top panel), *GW*@PBE0+BSE (middle panel), and PBE0+TDPBE0 (bottom panel). The results obtained within the corresponding independent particle approximation, i.e., ignoring electron-hole interaction, are also reported (dashed lines). Curves are vertically shifted for clarity. Bright and dark excitons energies are reported as vertical ticks.

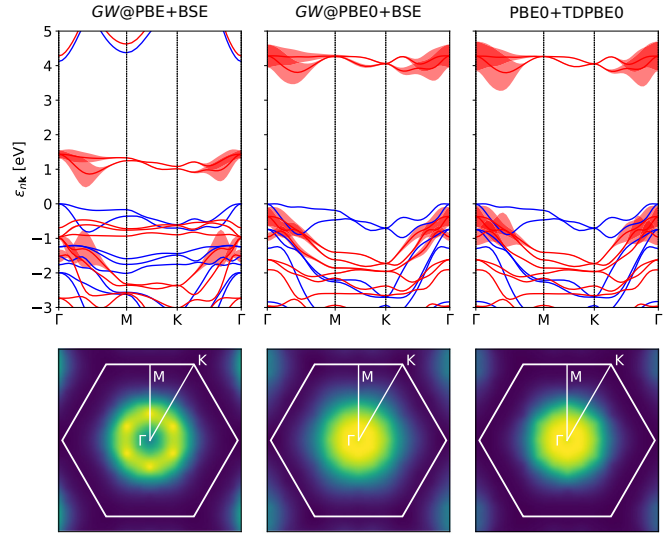

FIG. 3. Band contribution to the main excitonic peak E_0: (left panel) *GW*@PBE+BSE, (middle panel) *GW*@PBE0+BSE, (right panel) PBE0+TDPBE0. Note that the plotted band structures are the DFT ones. We also report the excitonic wave function in reciprocal space.

GW@PBE+BSE, this leads to a series of three bright excitons to appear, which we label D_i in Fig. 2 following the choice done in Ref. [18]. These peaks are located at 1.67 eV (D_1), 1.98 eV (D_2), 2.21 eV (D_3). As already pointed out, the description of the occupied t_{2g} states is questionable in PBE, and so are the absorption features related to them. Indeed the series of the D peaks is missing within *GW*@PBE0+BSE and PBE0+TD-BPE0, where all $d(t_{2g}) \rightarrow d(e_g)$ transitions are dark. This is probably due to the fact that the PBE starting point mixes d and p bands character, while PBE0 does not.

Beside these aspects, we are here interested in discussing whether or not $NiBr_2$ is an HEI. We thus need to turn our attention to the lowest-energy solutions among the $d(t_{2g}) \rightarrow d(e_g)$ transitions. As discussed, the occupied $d(t_{2g})$ states are very close to the valence band maximum within *GW*@PBE, while they are deeper in energy within PBE0 and *GW*@PBE0. As a consequence the *GW*@PBE+BSE approach produces negative eigenvalues. There is a doubly degenerate dark exciton at -0.17 eV ($X_{1,1}$) and a nondegenerate exciton at -0.16 eV ($X_{1,2}$). These two excitons share a similar physics and are labeled as X_1 in Fig. 2. Other two dark excitons located at 0.59 ($X_{2,1}$) and 0.68 eV ($X_{2,2}$) are indicated with X_2. Both X_1 and X_2 are associated with transitions between t_{2g} and e_g bands in the minority channel (see Supplemental Material [38]). The X_1 poles in particular are the ones which were used to claim the possible existence of an HEI ground state in Ref. [18]. Instead, within *GW*@PBE0+BSE and PBE0+TD-BPE0 no negative eigenvalues appear and therefore there is no EI phase. Since the qualitative behavior of these three approaches is the same, and, as discussed in Sec. I, the existence of a possible EI phase is mostly quantitative, we have now to address the question: which result is the most reliable? Both *GW*@DFT+BSE schemes are based on a one-shot *GW* calculation and plagued by inconsistencies between the approximation used for the ground state and the approximation used for the excited states. This points to the fact that, as far as this quantitative question is concerned, PBE0+TDPBE0 is the scheme to rely on. For $NiBr_2$ it should be noticed that the *GW*@DFT+BSE inconsistency is not so drastic. Indeed the physics of both the ground state and the excited states is determined by the same screened interaction W. However, the state-of-the-art *GW*@PBE+BSE is affected by a bad description of the occupied d bands in the current study, which is here crucial to address this quantitative answer. *GW*@PBE0+BSE suffers from a PBE0 screening, which is likely underestimated, although errors induced in the band structure are canceled by the overestimation of the binding energy, thus affecting in a less severe way the final position of the BSE peaks. We also notice that in Ref. [18], the HEI phase is also supported by HSE0+BSE simulations where, however, the inconsistency between ground-state and excited-states approximation is more problematic. Indeed it is noteworthy that BSE should be performed with quasiparticles, while HSE0 is more appropriate in a density functional context. TDHSE0 would be more methodologically sound.

In conclusion, our analysis of the band structure and the of the optical spectral features indicates that PBE0+TDPBE0 gives a good overall description of $NiBr_2$. Since this scheme does not produce any negative-energy pole in the optical absorption, we conclude that $NiBr_2$ is not an HEI. This is the most important result of this work.

IV. CONCLUSIONS AND PERSPECTIVES

In this work we addressed the study of excitonic insulator phases within common *ab initio* theoretical approaches such as time-dependent density functional theory and the Bethe-Salpeter equation of many-body perturbation theory. We discussed the fact that in order to correctly capture this phase a theoretical approach should be able to describe two important features, i.e., an electronic-driven broken symmetry and the long-range electron-hole interaction. That is why TDDFT within the common LDA/GGA approximations (which miss the long-range electron-hole interaction) cannot correctly describe this phase. The BSE is more appropriate, but, in order to correctly describe an electronic-driven broken symmetry, it should be used within consistent approximations. We discussed that this corresponds to use the same level of approximation for the self-energy used in a self-consistent ground-state calculation and for the kernel of the BSE.

For the specific case of ferromagnetic $NiBr_2$, by comparing the optical spectrum and the energy position of the lowest-energy dark excitons obtained with different schemes, we arrived at the conclusion that the PBE0+TDPBE0 scheme is the most reliable, also because it uses the same level of approximation for the ground state and for the excited states. Within PBE0+TDPBE0 all dark poles have a positive energy, which indicates that $NiBr_2$ is not an HEI, contrary to previous assignments. Moreover, we find that the occurrence of negative energy peaks in the *GW*@PBE+BSE is due to the starting-point dependence of the *GW* scheme, rather than to the inconsistency between ground-state and excited-state approximations. Indeed, the PBE starting point gives a questionable description of the t_{2g} states, which leads, within *GW*@PBE, to t_{2g} bands located too high with respect to the occupied *p* states. This does not happen within PBE0 and *GW*@PBE0 (and also with respect to other approximations studied in the literature such as HSE0 and PBE+*U*). More in general, our study points to the fact that using consistent approximations in *ab initio* theories is of crucial importance in order to have reliable results.

ACKNOWLEDGMENTS

S.D. and P.R. would like to acknowledge financial support by the EUR grant NanoX ANR-17-EURE-0009 in the framework of the "Programme des Investissements d'Avenir" and by the ANR (Projects No. ANR-18-CE30-0025 and No. ANR-19-CE30-0011). A.M.-S. acknowledge financial support by Ramón y Cajal programme (Grant No. RYC2018-024024-I; MINECO, Spain), Agencia Estatal de Investigación (AEI), through the Project No. PID2020-112507GB-I00 (Novel quantum states in heterostructures of 2D materials), and Generalitat Valenciana, program SEJIGENT (Reference No. 2021/034), project Magnons in magnetic 2D materials for a novel electronics (2D MAGNONICS), and Planes complementarios de I+D+I en materiales avanzados, Project SPINO2D, Reference No. MFA/2022/009. D.S. acknowledges the European Union project: MaX Materials design at the eXascale H2020-INFRAEDI-2018-2020, Grant Agreement No. 824143, and NFFA-Europe-Pilot project H2020-INFRAIA-2018-202 (Grant Agreement No. 101007417). D.S. acknowledges PRIN Grant No. 20173B72NB from MIUR (Italy).

[1] D. Jérome, T. M. Rice, and W. Kohn, Phys. Rev. **158**, 462 (1967).
[2] B. Bucher, P. Steiner, and P. Wachter, Phys. Rev. Lett. **67**, 2717 (1991).
[3] F. X. Bronold and H. Fehske, Phys. Rev. B **74**, 165107 (2006).
[4] H. Cercellier, C. Monney, F. Clerc, C. Battaglia, L. Despont, M. G. Garnier, H. Beck, P. Aebi, L. Patthey, H. Berger, and L. Forró, Phys. Rev. Lett. **99**, 146403 (2007).
[5] J.-J. Su and A. H. MacDonald, Nat. Phys. **4**, 799 (2008).
[6] Y. Wakisaka, T. Sudayama, K. Takubo, T. Mizokawa, M. Arita, H. Namatame, M. Taniguchi, N. Katayama, M. Nohara, and H. Takagi, Phys. Rev. Lett. **103**, 026402 (2009).
[7] S. S. Ataei, D. Varsano, E. Molinari, and M. Rontani, Proc. Natl. Acad. Sci. USA **118**, e2010110118 (2021).
[8] D. Varsano, S. Sorella, D. Sangalli, M. Barborini, S. Corni, E. Molinari, and M. Rontani, Nat. Commun. **8**, 1461 (2017).
[9] M. Hellgren, J. Baima, and A. Acheche, Phys. Rev. B **98**, 201103(R) (2018).
[10] K. Sugimoto, S. Nishimoto, T. Kaneko, and Y. Ohta, Phys. Rev. Lett. **120**, 247602 (2018).
[11] S. Dong and Y. Li, Phys. Rev. B **102**, 155119 (2020).
[12] Z. Jiang, W. Lou, Y. Liu, Y. Li, H. Song, K. Chang, W. Duan, and S. Zhang, Phys. Rev. Lett. **124**, 166401 (2020).
[13] G. Mazza, M. Rösner, L. Windgätter, S. Latini, H. Hübener, A. J. Millis, A. Rubio, and A. Georges, Phys. Rev. Lett. **124**, 197601 (2020).
[14] E. Baldini, A. Zong, D. Choi, C. Lee, M. H. Michael, L. Windgaetter, I. I. Mazin, S. Latini, D. Azoury, B. Lv, A. Kogar, Y. Wang, Y. Lu, T. Takayama, H. Takagi, A. J. Millis, A. Rubio, E. Demler, and N. Gedik, arXiv:2007.02909.
[15] B. Sun, W. Zhao, T. Palomaki, Z. Fei, E. Runburg, P. Malinowski, X. Huang, J. Cenker, Y.-T. Cui, J.-H. Chu, X. Xu, S. S. Ataei, D. Varsano, M. Palummo, E. Molinari, M. Rontani, and D. H. Cobden, Nat. Phys. **18**, 94 (2022).
[16] D. Chen, Z. Lian, X. Huang, Y. Su, M. Rashetnia, L. Ma, L. Yan, M. Blei, L. Xiang, T. Taniguchi, K. Watanabe, S. Tongay, D. Smirnov, Z. Wang, C. Zhang, Y.-T. Cui, and S.-F. Shi, Nat. Phys. **18**, 1171 (2022).
[17] L. Windgätter, M. Rösner, G. Mazza, H. Hübener, A. Georges, A. J. Millis, S. Latini, and A. Rubio, npj Comput. Mater. **7**, 210 (2021).
[18] Z. Jiang, Y. Li, W. Duan, and S. Zhang, Phys. Rev. Lett. **122**, 236402 (2019).

[19] M. C. T. D. Müller, Ph.D. thesis, Aachen University, 2017, https://publications.rwth-aachen.de/record/690012/files/690012.pdf.
[20] J. Koskelo, L. Reining, and M. Gatti, arXiv:2301.00474.
[21] Y. Tokunaga, D. Okuyama, T. Kurumaji, T. Arima, H. Nakao, Y. Murakami, Y. Taguchi, and Y. Tokura, Phys. Rev. B **84**, 060406(R) (2011).
[22] K. Riedl, D. Amoroso, S. Backes, A. Razpopov, Thi Phuong Thao Nguyen, K. Yamauchi, P. Barone, S. M. Winter, S. Picozzi, and R. Valentí, Phys. Rev. B **106**, 035156 (2022).
[23] Q. Song, C. A. Occhialini, E. Ergeçen, B. Ilyas, D. Amoroso, P. Barone, J. Kapeghian, K. Watanabe, T. Taniguchi, A. S. Botana, S. Picozzi, N. Gedik, and R. Comin, Nature (London) **602**, 601 (2022).
[24] X. Ma, G. Wang, H. Mao, Z. Yuan, T. Yu, R. Liu, Y. Peng, P. Zheng, and Z. Yin, Phys. Rev. B **105**, 035138 (2022).
[25] G. Lani, P. Romaniello, and L. Reining, New J. Phys. **14**, 013056 (2012).
[26] J. A. Berger, P. Romaniello, F. Tandetzky, B. S. Mendoza, C. Brouder, and L. Reining, New J. Phys. **16**, 113025 (2014).
[27] A. Stan, P. Romaniello, S. Rigamonti, L. Reining, and J. A. Berger, New J. Phys. **17**, 093045 (2015).
[28] M. C. T. D. Müller, C. Friedrich, and S. Blügel, Phys. Rev. B **94**, 064433 (2016).
[29] C. Friedrich, M. C. T. D. Müller, and S. Blügel, Many-body spin excitations in ferromagnets from first principles, in *Handbook of Materials Modeling : Methods: Theory and Modeling*, edited by W. Andreoni and S. Yip (Springer International Publishing, Cham, 2019), pp. 1–39.
[30] J. Paier, M. Marsman, and G. Kresse, Phys. Rev. B **78**, 121201(R) (2008).
[31] P. Giannozzi, S. Baroni, N. Bonini, M. Calandra, R. Car, C. Cavazzoni, D. Ceresoli, G. L. Chiarotti, M. Cococcioni, I. Dabo, A. D. Corso, S. de Gironcoli, S. Fabris, G. Fratesi, R. Gebauer, U. Gerstmann, C. Gougoussis, A. Kokalj, M. Lazzeri, L. Martin-Samos *et al.*, J. Phys.: Condens. Matter **21**, 395502 (2009).
[32] J. P. Perdew, K. Burke, and M. Ernzerhof, Phys. Rev. Lett. **77**, 3865 (1996).
[33] D. R. Hamann, Phys. Rev. B **88**, 085117 (2013).
[34] A. Marini, C. Hogan, M. Grüning, and D. Varsano, Comput. Phys. Commun. **180**, 1392 (2009).
[35] D. Sangalli, A. Ferretti, H. Miranda, C. Attaccalite, I. Marri, E. Cannuccia, P. Melo, M. Marsili, F. Paleari, A. Marrazzo, G. Prandini, P. Bonfà, M. O. Atambo, F. Affinito, M. Palummo, A. Molina-Sánchez, C. Hogan, M. Grüning, D. Varsano, and A. Marini, J. Phys.: Condens. Matter **31**, 325902 (2019).
[36] R. W. Godby and R. J. Needs, Phys. Rev. Lett. **62**, 1169 (1989).
[37] C. A. Rozzi, D. Varsano, A. Marini, E. K. U. Gross, and A. Rubio, Phys. Rev. B **73**, 205119 (2006).
[38] See Supplemental Material at http://link.aps.org/supplemental/10.1103/PhysRevB.107.115121 for details of the *GW* convergence, projected density of states and the analysis of excitons.
[39] R. M. Martin, L. Reining, and D. M. Ceperley, *Interacting Electrons: Theory and Computational Approaches* (Cambridge University Press, Cambridge, 2016).
[40] M. Rohlfing and S. G. Louie, Phys. Rev. B **62**, 4927 (2000).
[41] G. Strinati, Riv. Nuovo Cimento **11**, 1 (1988).
[42] M. R. Filip, J. B. Haber, and J. B. Neaton, Phys. Rev. Lett. **127**, 067401 (2021).
[43] A. Guandalini, P. D'Amico, A. Ferretti, and D. Varsano, arXiv:2205.11946.
[44] Computational 2D materials database (C2DB).
[45] M. Mushtaq, Y. Zhou, and X. Xiang, RSC Adv. **7**, 22541 (2017).
[46] F. Fuchs, J. Furthmüller, F. Bechstedt, M. Shishkin, and G. Kresse, Phys. Rev. B **76**, 115109 (2007).
[47] L. Leppert, T. Rangel, and J. B. Neaton, Phys. Rev. Mater. **3**, 103803 (2019).
[48] S. E. Gant, J. B. Haber, M. R. Filip, F. Sagredo, D. Wing, G. Ohad, L. Kronik, and J. B. Neaton, Phys. Rev. Mater. **6**, 053802 (2022).
[49] D. Bikaljević, C. González-Orellana, M. Peña-Diaz, D. Steiner, J. Dreiser, P. Gargiani, M. Foerster, M. A. Niño, L. Aballe, S. Ruiz-Gomez, N. Friedrich, J. Hieulle, L. Jingcheng, M. Ilyn, C. Rogero, and J. I. Pascual, ACS Nano **15**, 14985 (2021).
[50] F. Hüser, T. Olsen, and K. S. Thygesen, Phys. Rev. B **88**, 245309 (2013).